Effect of Cavitation on the Structure of Tip Leakage Vortex in an Axial Water-Jet Pump

Mohammad Hossein Arabnejad*, Arash Eslamdoost*, Urban Svennberg† and Rickard E. Bensow*

*Chalmers University of Technology, Gothenburg, Sweden, † Kongsberg Maritime Sweden AB, Kristinehamn, Sweden

mohammad.h.arabnejad@chalmers.se.

1 Introduction

Water-jet propulsion systems with axial pumps are mostly used in high-speed vessels and vessels designed for shallow water operations. To achieve high performance in these systems, the pump often operates in cavitating conditions. One type of cavitation in water-jet pumps is cavitation occurring in Tip Leakage Vortex (TLV), a vortex formed due to a leakage flow in the gap region between the tip of a rotating impeller blade and the stationary shroud casing. As the formation of cavitating TLVs is associated with a higher risk of erosion near the blade tip and higher level of vibration and noise [1, 2], it is of interest to understand the structure of TLV and how it is affected by cavitation.

Experimental methods have been used to study TLV in water jet pumps. Wu et al. [3, 4] and Miorini et al. [5] investigated the flow structures and turbulence of TLV formed in an axial water jet pump using Particle Image Velocimetry (PIV) measurements. They showed that TLV originates from vortical structures shed from the blade tip. These structures wrap around each other and form the core of the TLV. As the main vortex migrates in the blade passage, it becomes stronger due to the entrainment of vortical structures. Tan et al. [6, 7] showed that cavitation can incept in the form of bubble cavitation at the core of the TLV. They also showed that by lowering cavitation number, sheet cavitation with unsteady closure line can appear on the suction side of the rotor blade.

In addition to experimental methods, a few number of numerical studies have been devoted to studying the non-cavitating and cavitating TLV in water-jet pumps. For example, Zhang et al. [8, 9] examined the structure of non-cavitating and cavitating TLVs at different flow rates and cavitation numbers. All of these numerical studies used Reynolds Averaged Navier Stokes (RANS) approach, which requires an ad-hoc modification to be able to predict the correct cavitation dynamics [10]. Furthermore, experimental studies by Wu et al. [4] have shown that the flow in the TLV is anisotropic and is controlled by several interacting shear layers. Capturing the dynamics of these shear layers and the correct behavior of non-cavitating and cavitating TLV requires a scale-resolving approach, such as Large Eddy Simulation (LES). In this study, the flow in an axial water-jet pump, AxWJ-2 [11], is studied using an LES approach. The simulations are performed for both non-cavitating and cavitating conditions and the predicted performance and cavitation patterns are compared with the experimental data by Tan et al. [7]. Then, the numerical results are used to study the effect of cavitation on the structure of the TLV.

2 Numerical Set-up

In this study, a modified version of the interPhaseChangeFoam solver from the OpenFOAM-2.2.x framework [12] is used to obtain the numerical results. The turbulence modeling is achieved using LES where a low-pass filter is applied to the governing equations. This filtering results in the sub-grid-scale terms in the momentum equations which are, here, modeled using the wall-adapting local eddy-viscosity (WALE) model proposed by Nicoud and Ducros [13]. For cavitating simulation, the cavitation dynamics is captured by Transport Equation Modelling (TEM), where a transport equation for the liquid volume fraction, α^l, is solved. This equation has source terms accounting for vaporization and condensation, which are modeled using Schnerr-Sauer cavitation model [14].

In this paper, the AxWJ-2 axial water-jet pump [11] from the Johns Hopkins University is selected for the simulations. A sketch of this pump and a summary of its relevant data are given respectively in Fig. 1 and Table 1.

Table 1: Summary of relevant data for AxWJ-2 axial water-jet pump

D_1	305.2 mm
D_2	213.4 mm
D_{rotor}	303.8 mm
Number of rotor blades n_R	6
Number of stator blades n_S	8
Nominal tip clearance h	0.7 mm
Angular speed of the rotor Ω	900 RPM

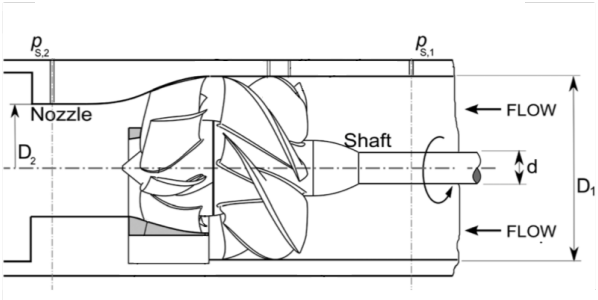

Fig. 1: Sketch of the AxWJ-2 axial water-jet pump [7]

Fig. 2a shows the computational domain used in this study. The computational domain is extended $10D_1$ upstream and downstream of the pump to reduce the interaction between the flow in the pump and the inlet and outlet boundary conditions. The domain is divided into three regions, inlet_pipe, rotor, and stator_outlet_pipe. Cyclic AMI interfaces are used for the boundaries between these regions. For the inlet_pipe, a fully structure grid is used. The mesh topology in the rotor region is shown in Fig. 2b. The mesh is divided into two regions with different types of mesh. The regions near the rotor blades, the hub, and the shroud are discretized with a structured hexahedral mesh, and the region in the middle of the passage is discretized with an unstructured mesh. To increase the mesh resolution in the tip leakage region, the resolution of this region for one blade is refined locally using refineHexMesh utility in OpenFOAM. The size of the refinement region relative to the radius of the pump is shown in Fig. 2b.

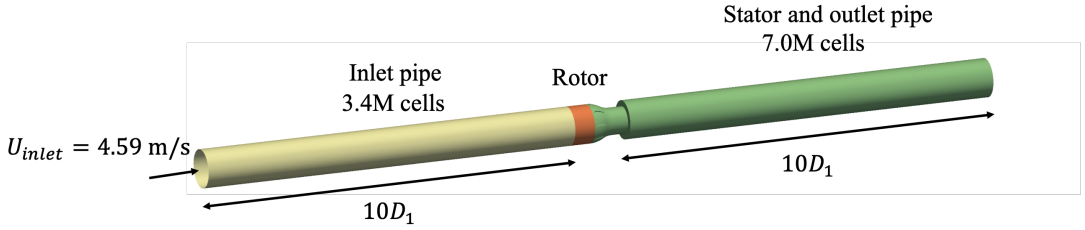

(a)

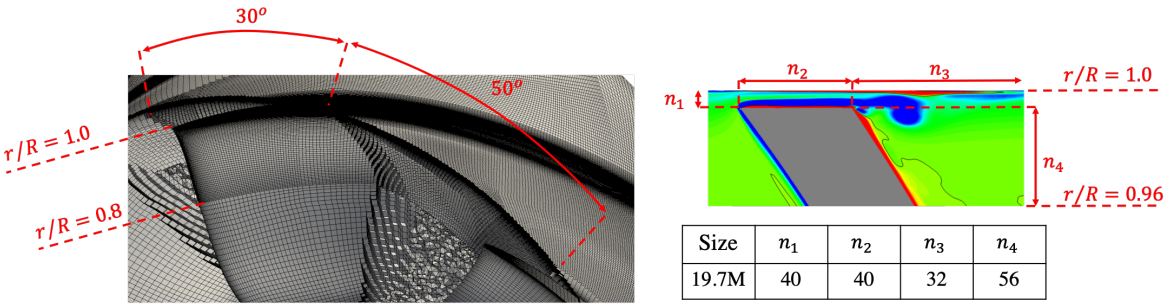

Size	n_1	n_2	n_3	n_4
19.7M	40	40	32	56

(b)

Fig. 2: a) Computational domain used in this paper, b) Mesh topology in the rotor region

3 Results

In the first part of the results, the predicted performance and cavitation pattern in the numerical simulation are compared with the experimental data by Tan et al. [7]. These authors reported the pump performance by two non-dimensional numbers, flow coefficient, φ, and head rise coefficient, ψ, which are defined as,

$$\varphi = \frac{Q}{nD_1^3}\ ,\ \psi = \frac{p_{s,2} - p_{s,1} + \frac{\rho}{2}\left[\left(\frac{Q}{A_2}\right)^2 - \left(\frac{Q}{A_1}\right)^2\right]}{\rho n^2 D_1^2}, \tag{1}$$

where Q is the volumetric flow rate in m^3/s and n is the shaft rotation speed in revolutions per seconds, and $p_{s,1}$, $p_{s,2}$, A_1, and A_2 are, respectively, the static pressures near the casing wall and the flow cross sections at location 1 and location 2, shown in Fig. 1. In this paper, we studied the pump at the flow coefficient, $\varphi = 0.75$. At this flow rate, the experimentally measured head rise coefficient, $\psi_{Exp.}$ is equal to 2.46. In table 2, the performance of the pump predicted by numerical simulations is compared with the experimental data. This comparison shows a good agreement between the predicted head-rise coefficient and experimentally measured one. It can also be concluded from table 2 that the effect of cavitation on the predicted performance at the cavitating condition studied here ($\sigma = 0.162$) is insignificant. This is expected as this condition is far away from the the cavitation breakdown according to Tan et al. [7].

Table 2: Performance of the pump predicted by numerical simulations

Simulations	σ	M_p	M_v	$M_{tot.}$	$\psi_{num.}/\psi_{exp.}$
Non Cavitating	∞	57.8	0.65	58.5	0.999
Cavitating	0.162	60.8	0.65	61.5	0.993

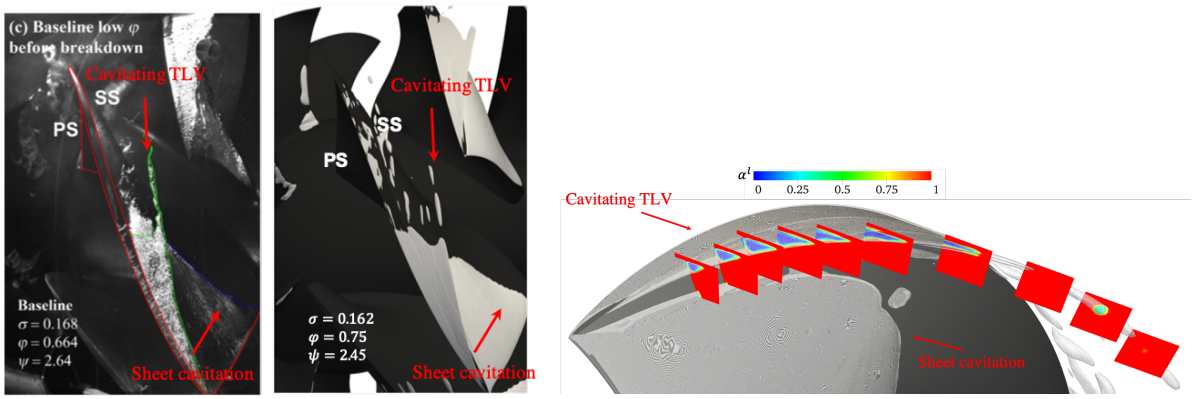

(a) HSV **(b)** Cavitating simulation

Fig. 3: Cavitating regions in a) High Speed Visualization (HSV) by Tan et al. [7] and b) Cavitating simulation (Cavitating regions are shows by an iso-surface of liquid volume fraction, α^l)

Fig. 3 shows the cavitation pattern captured by numerical simulation and the one in the experimental high speed visualization (HSV) by Tan et al. [7]. In the experiment, two main cavitating regions can be seen, sheet cavity formed on the suction side of the blade and the cavitating TLV. Comparison between numerical results and HSV shows that these cavitating region can be captured very well with the numerical simulation. From the distribution of liquid volume fraction on meridional planes in Fig. 3b, it can be seen that the cavitating TLV becomes thinner as it travels in the passage and that some cavitating vortices are detached from the trailing edge of the cavitating TLV. There is a also gap between cavitating TLV and sheet cavitation which indicates that the pressure in this region is higher than vapour pressure. This high pressure is due to the collision between the flow rotating around the cavitating TLV and the suction side of the blade. It can also be noted that the closure region of the sheet cavitation is unsteady and a vapour structure can be detached from the closure region due to this unsteadiness. Being able to capture this detachment is important as it has been shown in the previous studies that the detached cavity structures are associated with high risk of cavitation erosion [15].

In order to compare the structure of non-cavitating and cavitating TLV in the numerical simulations, the averaged tangential vorticity fields on several meridional planes are shown in Fig. 4. Three regions with high vorticity generation can be seen in the non-cavitating simulation. These regions are denoted by A, B, and C in Fig. 4a. Similar tangential vorticity distribution has been observed by Wu et al. [4] who showed that the high vorticity value in regions A, B, and C are, respectively, due to the shear layer between the reverse flow exiting the tip gap and the flow inside the passage, the boundary layer separation in the tip leakage flow near the rotor casing, and the core of the TLV. It can be seen in Fig. 4a that as

the main core of TLV (region C in Fig. 4a) develops in the passage, it detaches from the shear layer at the edge of the blade and the tangential vorticity in its centre decays. Comparison between Fig. 4a and 4b shows that the structure of the cavitating TLV is quite different from the non-cavitating one. In the first seven planes where cavitation exists according to Fig. 3b, a high value of vorticity occurs at the interface of the cavitating region instead of the centre of the cavitating TLV. No sign of the boundary layer detachment can be seen in these planes. However, in the last three planes, where a cavitating vortex is detached from the trailing edge of the cavitating TLV, the distribution of the averaged tangential vorticity is similar to the one in the non-cavitating TLV. In this region, the high value of tangential vorticity occurs in the detached vortex (region C in Fig. 4b) and the boundary layer detaches from the casing (region B in Fig. 4b). Similar to the non-cavitating TLV, the decay of tangential vorticity can be seen when the detached vortex travels in the passage.

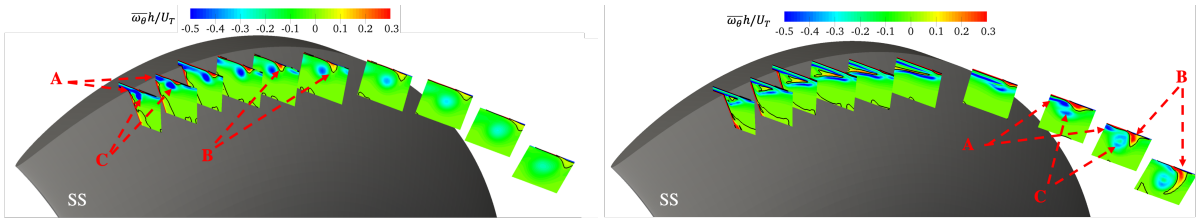

(a) $\sigma = \infty$ **(b)** $\sigma = 0.162$

Fig. 4: Comparison between the averaged tangential vorticity field on several meridional planes in non-cavitating and cavitating simulations (ω_θ: tangential vorticity, U_T: tangential velocity of the blade tip, h: tip gap height).

Fig. 5a and 5b show the distribution of averaged tangential velocity on several meridional planes in non-cavitating and cavitating simulations. In Fig. 5a, it can be seen that as the non-cavitating TLV travels downstream, the averaged tangential velocity increases around the centre of vortex. This increase occurs in the planes where averaged tangential vorticity in the core of the TLV decays (region B) in Fig. 4a. Wu et al. [4] postulated that both the increase in tangential velocity and the decay of tangential vorticity are due to the bursting of the TLV core. To confirm this, Fig. 5c shows an iso-surface of the Q criteria colored by the instantaneous tangential velocity in the non-cavitating simulation. It can be seen that the centre-line of the TLV is almost a straight line in the first five meridional planes and the tangential velocity is small around the TLV. As the vortex becomes unstable and its centre-line deviates from the straight line, spots with a high value of tangential velocity can be seen around the vortex. These spots, marked as region A in Fig. 5c, occur at the planes where the increase in average tangential velocity and the decay of tangential vorticity can be seen. Fig. 5b shows the averaged tangential velocity in the cavitating simulation. It can be seen that the tangential velocity in the cavitating region of TLV (first five planes in Fig. 5b) is high which means that the cavitating region rotates with the blade rotational speed. This is different from the non-cavitating TLV where the averaged tangential velocity is low in the first five planes in Fig. 5a. In the last three planes in Fig. 5b, where a cavitating vortex is detached from the edge of the cavitating TLV, the average tangential velocity is low around the core of cavitating vortex and it increases as the vortex travels in the passage which is similar to non-cavitating TLV. Fig. 5d shows an iso-surface of the Q criteria colored by the instantaneous tangential velocity in cavitating simulation. No vortical structure can be seen in the cavitating part of TLV and spots with high tangential velocity can seen when the centre-line of the cavitating vortex in the last three planes deviates from a straight line.

4 Conclusions

In this paper, we present LES results of non-cavitating and cavitating flows in an axial water-jet pump with the aim to study the effect of cavitation on the TLV. First, we compare the predicted performance and cavitation patterns with the experimental data by Tan et al. [7] and this comparison shows a very good agreement. Then, we investigate the structure of non-cavitating and cavitating TLVs by analyzing numerical results. Our results show that the structure of TLV is highly affected by the presence of cavitation. In the cavitating TLV, the high value of vorticity mostly occurs at the interface of the cavitating

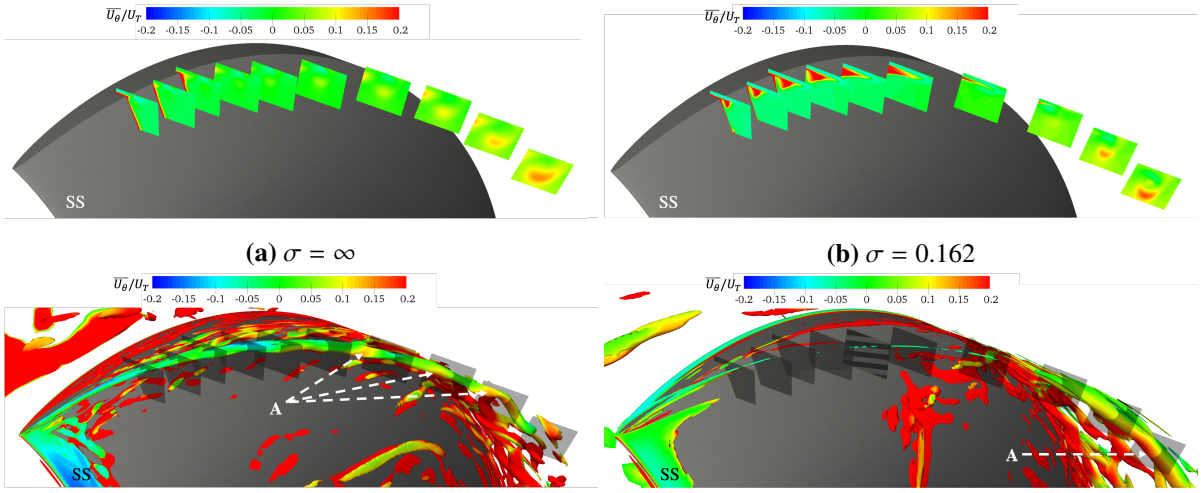

(a) $\sigma = \infty$ **(b)** $\sigma = 0.162$

(c) $\sigma = \infty$ **(d)** $\sigma = 0.162$

Fig. 5: Comparison between the normalized averaged tangential velocity and iso-surface of Q criteria colored by instantaneous tangential velocity in non-cavitating and cavitating simulations (U_θ: tangential velocity, U_T: tangential velocity of the blade tip)

region while in the non-cavitating TLV, a high value of vorticity can be seen in three regions, the shear layer between the reverse flow exiting the tip gap and the flow inside the passage, the boundary layer separation in the tip leakage flow near the rotor casing, and the core of the TLV. Furthermore, our cavitating simulations show that a cavitating vortex is detached from the trailing edge of the cavitating TLV. As this vortex travels in the passage, the averaged tangential vorticity in the vortex decays and the average tangential vorticity increases. Similar phenomena can be seen in the non-cavitating TLV and it is shown that these phenomena are due to the bursting of the vortex.

Acknowledgements

Financial support for this work has been provided by Kongsberg Maritime through the University Technology Centre in Computational Hydrodynamics hosted at the Division of Marine Technology, Department of Mechanics and Maritime Sciences at Chalmers. The simulations were performed on resources at Chalmers Centre for Computational Science and Engineering (C3SE) provided by the Swedish National Infrastructure for Computing (SNIC).

References

R. Laborde, P. Chantrel, and M. Mory, "Tip clearance and tip vortex cavitation in an axial flow pump," *Journal of Fluids Engineering*, vol. 119, no. 3, pp. 680–685, 1997.

F. Avellan, "Introduction to cavitation in hydraulic machinery," in *The 6th International Conference on Hydraulic Machinery and Hydrodynamics, Timisoara, Romania*, 2004, pp. 21–22.

H. Wu, D. Tan, R. Miorini, and J. Katz, "Three-dimensional flow structures and associated turbulence in the tip region of a waterjet pump rotor blade," *Experiments in Fluids*, vol. 51, no. 6, pp. 1721–1737, 2011.

H. Wu, R. L. Miorini, D. Tan, and J. Katz, "Turbulence within the tip-leakage vortex of an axial waterjet pump," *AIAA Journal*, vol. 50, no. 11, pp. 2574–2587, 2012.

R. Miorini, H. Wu, and J. Katz, "The internal structure of the tip leakage vortex within the rotor of an axial waterjet pump," *Journal of Turbomachinery*, vol. 134, no. 3, p. 031018, 2012.

D. Tan, R. Miorini, J. Keller, and J. Katz, "Flow visualization using cavitation within blade passage of an axial waterjet pump rotor," in *ASME 2012 Fluids Engineering Division Summer Meeting collo-*

cated with the ASME 2012 Heat Transfer Summer Conference and the ASME 2012 10th International Conference on Nanochannels, Microchannels, and Minichannels. American Society of Mechanical Engineers, 2012, pp. 395–404.

D. Tan, Y. Li, I. Wilkes, E. Vagnoni, R. Miorini, and J. Katz, "Experimental investigation of the role of large scale cavitating vortical structures in performance breakdown of an axial waterjet pump," *Journal of Fluids Engineering*, vol. 137, no. 11, p. 111301, 2015.

D. Zhang, W. Shi, B. van Esch, L. Shi, and M. Dubuisson, "Numerical and experimental investigation of tip leakage vortex trajectory and dynamics in an axial flow pump," *Computers & fluids*, vol. 112, pp. 61–71, 2015.

D. Zhang, W. Shi, D. Pan, and M. Dubuisson, "Numerical and experimental investigation of tip leakage vortex cavitation patterns and mechanisms in an axial flow pump," *Journal of Fluids Engineering*, vol. 137, no. 12, p. 121103, 2015.

O. Coutier-Delgosha, R. Fortes-Patella, and J. Reboud, "Evaluation of the turbulence model influence on the numerical simulations of unsteady cavitation," *Journal of Fluids Engineering*, vol. 125, no. 1, pp. 38–45, 2003.

T. Michael, S. Schroeder, and A. Becnel, "Design of the ONR AxWJ-2 axial flow water jet pump," Hydromechanics Department Report No. NSWCCD-50TR-2008/066., Tech. Rep., 2008.

H. Weller, G. Tabor, H. Jasak, and C. Fureby, "A tensorial approach to computational continuum mechanics using object-oriented techniques," *Computers in physics*, vol. 12, no. 6, pp. 620–631, 1998.

F. Nicoud and F. Ducros, "Subgrid-scale stress modelling based on the square of the velocity gradient tensor," *Flow, turbulence and Combustion*, vol. 62, no. 3, pp. 183–200, 1999.

J. Sauer, "Instationär kavitierende strömungen-ein neues modell, basierend auf front capturing (vof) und blasendynamik," *Diss., Uni Karlsruhe*, 2000.

M. Arabnejad, A. Amini, R. Bensow, and M. Farhat, "Experimental and numerical investigation of the cavitating flows over a modified NACA0009 foil," in *The 10th International Symposium on Cavitation (CAV2018), Baltimore, Maryland, USA*, 2018.